ACS APPLIED MATERIALS & INTERFACES

Research Article

www.acsami.org

Varying TiO_2 Macroscopic Fiber Morphologies toward Tuning Their Photocatalytic Properties

Natacha Kinadjian,[†,§] Mickaël Le Bechec,[‡] Catherine Henrist,[∥] Eric Prouzet,[§] Sylvie Lacombe,*[,‡] and Rénal Backov*[,†]

[†]Université de Bordeaux, Centre de Recherche Paul Pascal, office 115, UPR 8641-CNRS, 115 Avenue Albert Schweitzer, 33600 Pessac, France

[‡]IPREM-UMR CNRS 5254, Université de Pau et des Pays de l'Adour, Hélioparc-2 Av. du Président Angot, F-64053 Pau Cedex 09, France

[§]Department of Chemistry, University of Waterloo, 200 University Avenue West, Waterloo, Ontario, Canada N2L 3G1

[∥]University of Liège, Department of Chemistry, GREENMAT-LCIS, B6 Sart Tilman, 4000 Liege, Belgium

Supporting Information

ABSTRACT: In a context of volatile organic compound photodecomposition, we have addressed TiO_2-based macroscoscpic fiber generation. We have extruded hybrid sols of amorphous titania nanoparticles, latex nanoparticles, and nonionic surfactant (Tergitol) as structure-directing agents into a poly(vinyl alcohol) (PVA) solution bearing salts acting as a flocculating medium. The resulting nanocomposite TiO_2/latex/PVA macroscopic fibers were thermally treated in air to open porosity by organic removal while generating the photocatalytically active anatase phase of TiO_2 along with residual brookite. Considering the synthetic paths, we have varied both the diameter of the latex particles as well as their concentration within the starting sol. These parameters allow tuning both the voids created through the applied thermal treatment and the fiber final diameters. For gas-phase photocatalysis, we have shown that the fiber diameters, mesoscopic roughness, and macroscopic topological defects represent indeed important morphological parameters acting cooperatively toward both acetone degradation and its mineralization processes. Particularly, triggering the fiber morphological characteristics, we have increased their efficiency toward acetone degradation of around 550% when compared with previous work.

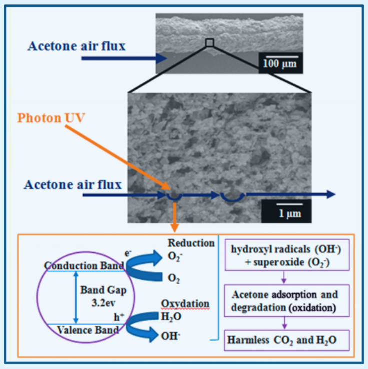

KEYWORDS: *photocatalysis, fibers, titania, porous matter, integrative chemistry, sol−gel*

INTRODUCTION

Titanium dioxide (TiO_2) is a typical n-type semiconductor accepted as an effective photocatalyst for the photooxidation of different kinds of hazardous organic pollutants in wastewater, drinking water, and air[1−7] because of its nontoxicity, chemical stability, and intrinsic band-gap energy (3.2 eV). The photocatalytic activity of TiO_2 is largely determined by its properties, such as specific surface area, crystallinity, crystalline size, and porous structure.[8−13] In addition, TiO_2 materials with a large surface area and high crystallinity always demonstrate enhanced activity for the degradation of environmental contaminants[14−16] because the large surface area can provide many active sites for adsorption of substances. Photocatalytic nanostructured TiO_2 may be prepared with various morphologies of nanostructured TiO_2, including nanoparticles, nanofibers, nanostructured films or coatings, and nanotubes.[17−31] The photocatalytic activity of TiO_2 is one of its distinctive features, mainly attributed to its anatase phase,[32,33] and it is reported that higher crystallinity drastically enhanced the photocatalytic activity of TiO_2 materials.[34,35] In addition to crystallinity, the efficiency of the photocatalyst will also depend on its specific surface area and, more specifically, on the way pollutants can reach the catalyst. From this point of view, 2D-mesoporous TiO_2 appears as an excellent candidate for this application,[36−38] but a number of recent works also focused on the fabrication of one-dimensional (1D) TiO_2 photocatalysts, with a special attention paid to TiO_2 nanotubes.[39−41] The large surface-to-volume ratio, the enhanced adsorption of various reactants, and the favorable morphology for enhancing a longer reactant−catalyst contact while optimizing mass transport are expected to improve, overall, the properties of these materials.[32] Among the techniques developed for the fabrication of macroscopic1D TiO_2 nanostructures, electrospinning offers several advantages, such as simplicity, process controllability, low production cost, and scalability for producing industrial quantities.[33,42−44] However, several penalties inherent to the electrospinning technique are the facts that native fibers are randomly dispersed during the synthesis step, resulting in a direct loss of unidirectionality at the macroscopic scale, final random fibers being not self-standing, but supported, while

Received: March 6, 2014
Accepted: June 20, 2014
Published: June 20, 2014

their macroscopic cohesion suffers from the sintering imposed during the thermal treatment. Furthermore, the fibers' random distribution from one experiment to another does not allow normalized photocatalytic efficiency as the resulting roughness and thickness are hardly controllable.

In this work, we studied more specifically the multiscale optimization, from porosity to surface roughness of these fibers. Designing such architectures can be addressed through an *Integrative Chemistry* pathway.[45−49] The concept of integrative chemistry was formalized 8 years ago as a interdisciplinary tool box, encompassing the domains of chemistry, biology, and physics of complex fluids, to design on demand advanced functional materials. It is, indeed, in this vein that the NSF did rely later on this interdisciplinary approach of materials science, under its Integrative Chemistry Activity (ICA) program. We have recently proposed titania macroscopic fiber generation achieved by an extrusion process[50] in the same way as the generation of vanadium oxide[51−55] and zinc oxide macroscopic composite fibers.[56] We demonstrated that the specific 1D shape design and surface mesocopic roughness of various nanoporous titania fibers can actually influence the photocatalytic properties, determined by gaseous acetone mineralization (i.e., decomposition into CO_2 and H_2O) in a specially designed reactor under unidirectional gas flow.

■ EXPERIMENTAL SECTION

Materials. Titanium isopropoxide, HCl (37 wt %), Tergitol NP-10 (a nonylphenol-EO_{10} nonionic surfactant), NH_4OH, and Na_2SO_4 were purchased from Aldrich and used as received. Poly(vinyl alcohol) (PVA) (M_w 195 000, hydrolyzed, 99%) was purchased from Fluka and used as received. Monodisperse polystyrene (PS) dispersions were prepared by emulsion polymerization according to the process described by Zhang et al.[57] Latex particles presenting diameters of 130 and 260 nm were synthesized for this study.

Syntheses. *TiO_2 Nanoparticles.* The nanoparticles were synthesized according to the process described in our previous work.[50] Typically, 5 mL of a HCl solution was first added to 50 mL of nonylphenol-EO_{10} nonionic surfactant (Tergitol NP-10; 15 wt %) solution. The pH of the solution was then increased up to 1.8 by addition of an ammonia solution. Titanium isopropoxide was then slowly added under stirring (6.4 mL), and the solution was left at room temperature. A slurry-like white precipitate was formed after 12 h, which was recovered after full evaporation. The resulting powder was washed several times with deionized water until no foaming resulting from the remaining surfactant was observed.

TiO_2/PVA/Latex Fibers Prepared by Coextrusion. First, aqueous suspensions of TiO_2 nanoparticles were prepared from the dry extracts in order to obtain 4 wt % in the final solution. Solid PVA was then added into the solution under stirring at 90 °C in a proportion of 1.2 g of PVA for 10 mL of solution. This solution was kept under stirring for 1 h until the PVA was fully dissolved and then cooled down at 60 °C. When the solution reached 60 °C, the latex particles were incorporated in the solution maintained under stirring. In order to ensure the homogeneity of the solution, the solution was then cooled down at room temperature and agitated with a vortex mixer. The fibers were then generated by needle injection (spinneret diameter of 500 μm) of the PVA/TiO_2/latex sols into a rotating bath (25 rpm) containing a saturated salt solution of Na_2SO_4 at 45 °C. The extrusion speed was set at 40 $mL \cdot h^{-1}$, and the flux was maintained tangential to the rotation axis of the beaker. Upon the completion of the extrusion process, the TiO_2/PVA/latex fibers were meticulously taken out of the beaker by hand and allowed to dry in air. Finally, the fibers were washed once in water to remove the excess of salt.

TiO_2 Fiber Sintering. The as-synthesized fibers were then sintered at 450 °C for 6 h in order to remove the organic part while promoting crystallization. Overall, 7 different inorganic fibers were prepared and labeled hereafter X-Y-TiO_2, where X denotes the diameter of the latex nanoparticles, and Y the latex particles' weight percentage related to TiO_2 in the sol. Thereby, we report in the following the comparison among several fibers, named as TiO_2, 130-10-TiO_2, 130-30-TiO_2, 130-60-TiO_2, 260-10-TiO_2, 260-30-TiO_2, and 260-60-TiO_2. The results were compared to our first results, where the fibers were extruded through a bigger needle (1 mm diameter) without latex in the starting solution. More specifically, it was compared to the 4-TERG-TiO_2 fibers, which will be referenced in this paper as "TiO_2 ref".[50]

Characterization. Scanning electron microscopy (SEM) observations were performed on a 6700F JEOL apparatus, which is a high-resolution model equipped with a cold cathode field emission gun. The working voltage was set up at 10 or 5 kV. Specific surface areas and pore characteristics at the mesoscale were measured using a nitrogen adsorption method with a Micromeritics ASAP 2010. The samples were outgassed at 150 °C under vacuum for 12 h before the measurement. Material roughness was evaluated from the determination of the fractal surface dimension (D_s), which can be deduced from the nitrogen isotherm adsorption curves. D_s was calculated according to the procedure described previously.[58] The experimental adsorption isotherm data are replotted according to the following development that can be found in detail elsewhere[59]

$$\theta = K[\log(P/P_0)] - \nu \tag{1}$$

where $\nu = 3 - D_s$, θ is the relative adsorption calculated by normalizing the curve with the highest adsorption value, K is a constant, and D_s is the surface fractal dimension that we are looking for. An easy way to obtain D_s is to convert eq 1 according to

$$\log(\theta) = \log(K) - \nu \log(\log[P/P_0]) \tag{2}$$

D_s is deduced from the slope of the line, and it must vary between 2 (flat surface) and 3. Any value higher than 2 describes an increasing surface roughness. The adsorption range to be used for this analysis has to be taken within the partial pressure range of $0.05 < P/P_0 < 0.3$ and limited below the Kelvin condensation step that corresponds to the pore filling.[59] The crystalline structure of TiO_2 was characterized by XRD with a PANalytical X'pert MDP with a Bragg−Brentano θ−θ geometry diffractometer, equipped with a back graphite monochromator and an Anton-Paar HTK 16 chamber (Cu Kα X-ray, $\lambda = 1.54$ Å, 40 kV working voltage, 50 mA working intensity).

Photocatalytic mineralization of gaseous acetone was carried out in a specially designed batch reactor (Scheme S.1, Supporting Information), based on a PTFE circulating loop where a photoreactor (1) was inserted. The gas was automatically and periodically sampled through a 10 $L \cdot min^{-1}$ pump to a Varian 3800 GC equipped with an FID detector (for volatile organic compound (VOC) monitoring) and a methanizer for CO_2 detection. The cylindrical photoreactor was a thermoregulated pyrex column where a pyrex canister (inner diameter 10 mm) containing the photocatalytic fibers was slipped. The air flow velocity is around 0.7 $m \cdot s^{-1}$ when the flow meter is set on 3.3 $L \cdot min^{-1}$. Four fluorescent tubes (Philips TLD8W) with an emission maximum at 366 nm were set upon the photoreactor, to deliver an irradiance of 3.2 $mW \cdot cm^{-2}$ UVA, measured with an International Light ILT900 Spectroradiometer. The irradiance actually received by the photocatalytic fibers in the reactor was reduced by the absorption of the two pyrex walls of the thermoregulated jacket of the reactor, and the pyrex canister containing the fibers. Photocatalytic activity of our samples was compared with Quartzel PCO from Saint-Gobain Quartz, under strictly identical conditions (reactor, lamps, flow rate, % RH, initial acetone concentration). A 24.8 mg portion of Quartzel, and 19.3−50.4 mg of laboratory-made fibers, were tested in the canister reactor. The ratio of remaining acetone is given per gram of photocatalytic media, even though it is known that Quartzel fibers are made of quartz fibers coated with TiO_2 (composition of the commercial product unknown, fiber diameters 9 μm, specific surface area 120 $m^2 \cdot g^{-1}$). For all the experiments, the same procedure was followed: once the reactor containing the photocatalytic media was settled in the device, synthetic air was introduced and the relative humidity was adjusted to 15% by injecting the required amount of water through a septum on top of the tank. The flow-rate of the circulation pump was 3.3 L min^{-1}, corresponding to a 0.7 m s^{-1} velocity of the gas on the photocatalytic media for reactors (it was previously verified on Quartzel fibers that this flow rate was optimal for acetone conversion). The temperature of the circulating gas was 22 ± 2 °C. The photocatalytic media were first irradiated for 20 h without acetone under these conditions in order to activate them and determine the possible evolution of adsorbed VOCs or CO_2. No peak appeared on the chromatograph during this step, but a slow CO_2 increase was noticed due to the leaks in the device and possibly to the photocatalytic degradation of residual organic materials contained within the fiber. The lamps were then switched off. Then, 45 ppmv (2 μL) of acetone was injected in the tank through the septum. The acetone adsorption step on the media was followed by GC. When the gaseous acetone concentration was stable, the lamps were switched on (time 0). Acetone and CO_2 concentration was monitored every 7 min by automatic sampling on the GC-FID-methanizer. The device leaks were determined by monitoring the CO_2 concentration in the dark for 20 h and by monitoring the acetone concentration for 10−20 h once it has been introduced into the system in the dark (less than 10% loss within 10 h). They were then subtracted for the results analyses.

■ RESULTS AND DISCUSSION

Fiber Syntheses and Characterization. The TiO_2/PVA/latex sols can be extruded as composite PVA/TiO_2/latex macroscopic fibers (Figure 1). Once these hybrid fibers had been synthesized, we applied thermal treatment to promote TiO_2 nanoparticle crystallization and sinter the materials while calcining the organic counterpart. We studied X-ray patterns in order to see if the introduction of latex particles influenced the crystalline phase of TiO_2. X-rays showed the same pattern for all types of fibers. The fibers are mainly composed of anatase phase with residual brookite, together with sharp peaks being related to Na_2SO_4 (Figure S.1, Supporting Information). SEM analyses allowed visualizing the distribution of particles and macropores after this thermal treatment. We observe that the diameter of the fibers varies from the simple to double. Indeed, when the amount of organic mold increases, the final fiber diameters decrease drastically. The diameters are ranging from 100 to 200 μm (Figure 1c−f).

The mesoporosity was studied by nitrogen adsorption on calcined fibers. All the materials exhibited a rather straight adsorption curve, which can be described as a type IV isotherm (Figure 2), and a pore size distribution within the mesoporous range (Figure 3).

The hysteresis observed is significant for the new synthesized fibers compared to the reference fibers,[50] indicating an increased mesoporosity for the latex-based fibers. The presence of steep adsorption at $P/P_0 < 0.05$ showed that the fibers were also microporous. The pore size distribution, calculated with the Barrett−Joyner−Halenda (BJH) equation from the desorption curves, indicated that the pore sizes were between 5 and 10 nm rather than 6 and 15 nm for the reference.[60] The specific surface areas of the titanium dioxide fibers are displayed in Table 1. All surface areas were in agreement with a pronounced mesoporosity. However, as for the pores size, the specific areas of the new fibers decreases compared to the reference fibers from 700 $m^2 \cdot g^{-1}$ to about 95 $m^2 \cdot g^{-1}$. Decreasing the diameter of the fibers from 400 μm[50] to 150 μm for the new fiber batches (bearing latex or not) addresses thus a strong impact over the specific surface area. This phenomenon can be explained by an exalted sintering process due to a smaller temperature gradient within the fibers bearing the smaller diameters.

In parallel, we analyzed the surface mesocopic roughness of these materials (Figure 4), as this feature can be an important factor in photocatalysis for an optimized interaction between the pollutants and the catalyst.[50] From Table 1, D_s was about 2.5 for the new latex fibers, which is significantly higher than the fibers of the previous study ($D_s = 2.3$).[50] Despite the similar values of the new fibers' mesoscopic roughness, the macroscopic topologies, with and without latex particles, are different (Figure 1). Consequently, these types of fibers will not necessarily present the same photocatalytic behavior, as the air convection flux is sensitive to the surface macroscopic topology.

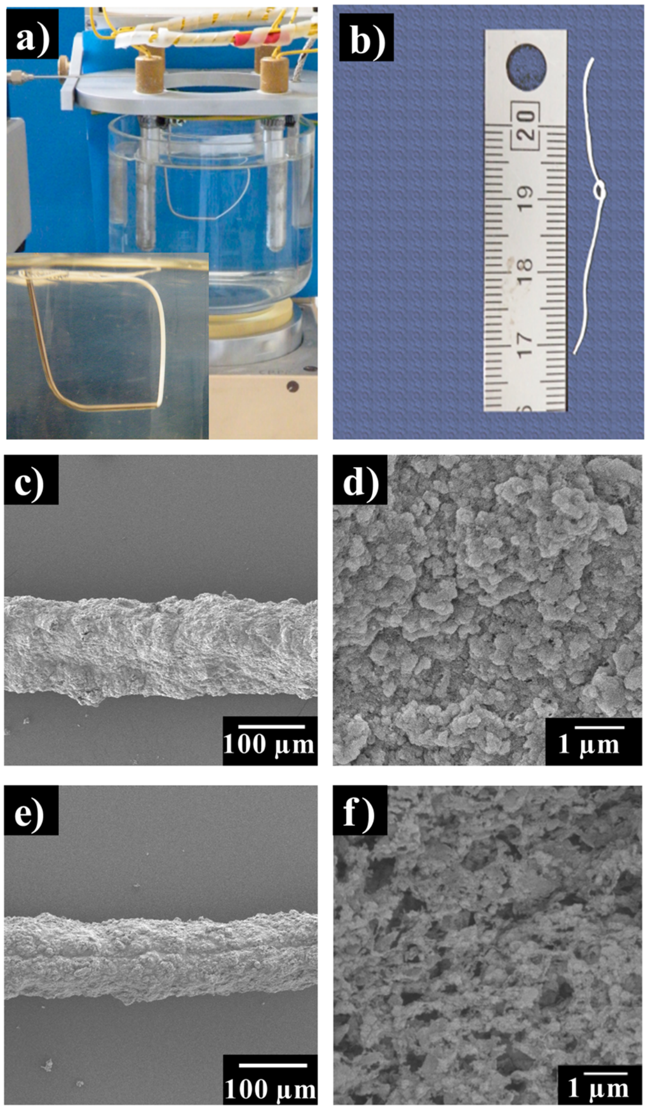

Figure 1. Pictures of TiO_2 fiber generation through extrusion process (a); a zoom over the extruded sol is proposed within the embedded image. (b) View of a fiber that we knotted. SEM pictures of calcined TiO_2 fibers (c, d) and of a 130-60-TiO_2 fiber (e, f).

Fibers Photocatalytic Efficiency. Gaseous acetone oxidation was chosen as a representative well-known photocatalytic test leading to mineralization.[61−63] However, to carry out the reaction with a parallel gas flow (uniaxial) toward the fibers' main axis, specific photocatalytic homemade Pyrex reactors containing a Pyrex canister were designed and introduced in the circulating loop (Scheme S.1, Supporting Information). The flow rate of the circulating synthetic air at 15% relative humidity (RH) was 3.3 L min^{-1} over the

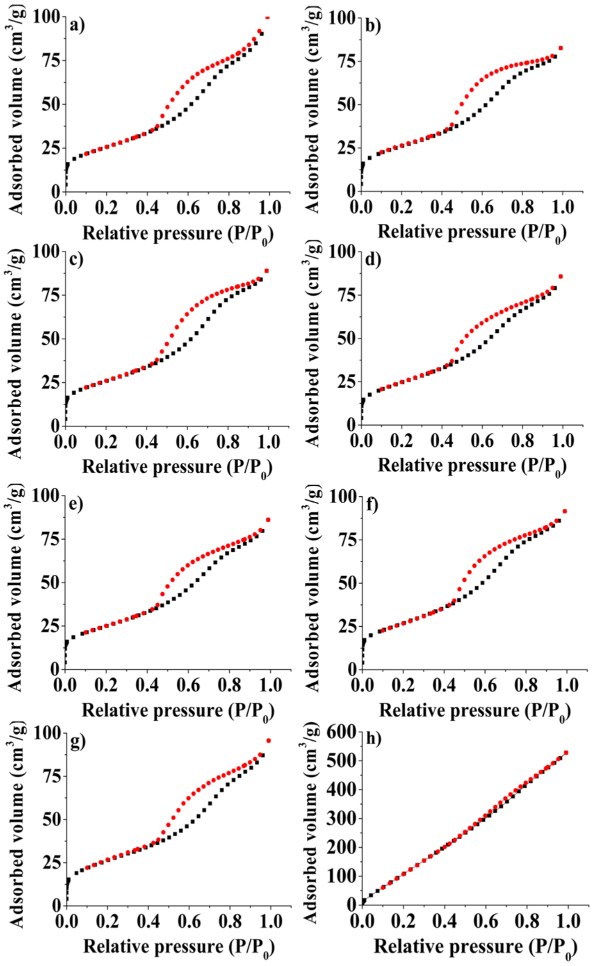

Figure 2. Nitrogen physisorption experiments: (■) adsorption curves, (●) desorption curves. (a) TiO_2, (b) 130-10-TiO_2, (c) 130-30-TiO_2, (d) 130-60-TiO_2, (e) 260-10-TiO_2, (f) 260-30-TiO_2, (g) 260-60-TiO_2, and (h) TiO_2 ref fibers, which are the fibers of reference from previous work.[50]

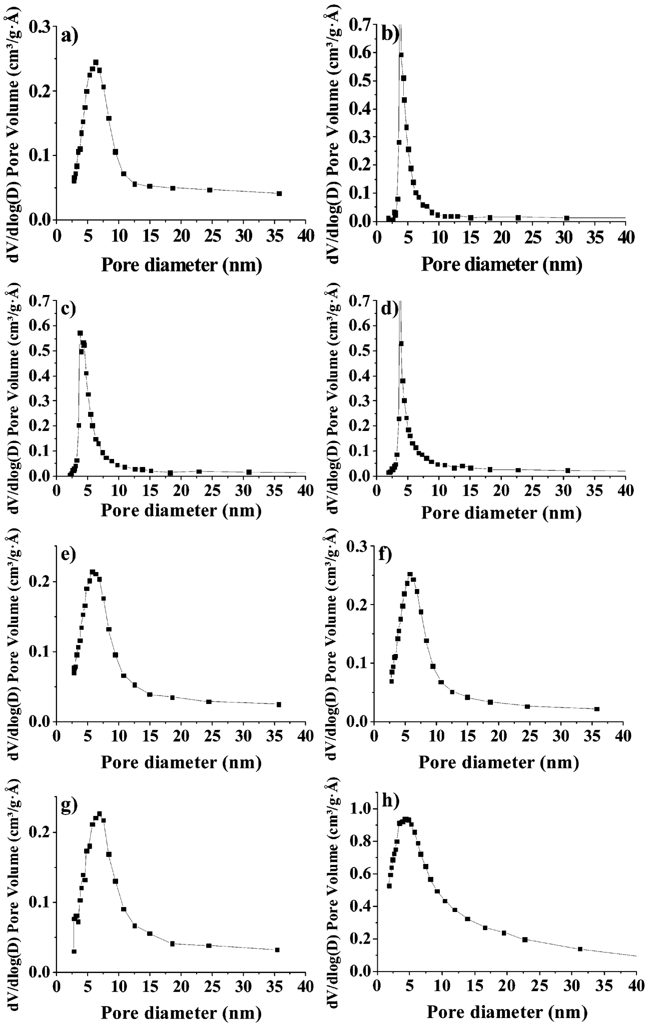

Figure 3. Pore size distribution deduced from nitrogen desorption curves: (a) TiO_2, (b) 130-10-TiO_2, (c) 130-30-TiO_2, (d) 130-60-TiO_2, (e) 260-10-TiO_2, (f) 260-30-TiO_2, (g) 260-60-TiO_2, and (h) TiO_2 ref fibers.

photocatalytic media, corresponding to an air velocity of 0.7$m \cdot s^{-1}$.

In a first step, the photocatalytic device and the reaction conditions were settled with commercial TiO_2 fibers (Quartzel PCO, Saint-Gobain Quartz) in the same configuration (canister and reactor). This commercial photocatalytic media is made of quartz fibers coated with TiO_2. The performances of the lab-made TiO_2 fibers were then compared to those of this highly efficient commercial material under identical conditions, with a first activation step under irradiation without acetone and a second step with injected acetone (50 ppmV) under identical flow rates, RH, and temperatures. Typical curves of acetone concentration per gram of photocatalytic media against time are compared Figure 5a. The first-order kinetic constants, *k*, calculated from the acetone degradation rate per gram of media, are given Figure 5c. (fitting of the ln curves in Figure S.2 (Supporting Information). A very positive result is the much higher efficiency of these new synthesized fibers relative to the previous TiO_{2ref} sample bearing both lower mesoscopic roughness and a larger diameter.[50]

These results show also that the specific surface area is not the crucial parameter under these conditions as the reference fibers present a much higher specific surface area (TiO_{2ref}, 700 $m^2 \cdot g^{-1}$) compared to that of the latex-based ones (88–96 $m^2 \cdot g^{-1}$). This result is consistent with our previous work where we could observe that, even though the specific surface area of the 4-TERG-TiO_2 (700 $m^2 \cdot g^{-1}$) was much higher than the one of 4-TTAB-TiO_2 (430 $m^2 \cdot g^{-1}$), the reaction kinetics were similar.[50] This phenomenon is certainly due to the experimental conditions as the photocatalytic tests are performed under uniaxial flux with a velocity of 0.7 $m \cdot s^{-1}$ where, in such hydrodynamic condition, the internal mesoscopic voids are certainly not completely involved within the photocatalysis reaction. Considering this result, as found by other groups,[64] we can deduce that mesoporosity is not of crucial importance when dealing with gas-based photocatalysis.

Beyond, we should not forget that the UV penetration depth is only around 100 nm[65] while the fiber diameters are about several hundred micrometers; thus, only a thin shell of the fiber is UV-activated. Consequently, the higher reaction kinetics of the new fibers, given per gram of media, also results from the diminution of the fibers' diameter. We can then conclude that the overall increase of the reaction kinetics between TiO_2 ref (0.007 $min^{-1} \cdot g^{-1}$) and TiO_2 fibers (0.028 $min^{-1} \cdot g^{-1}$) results from the cooperative effect between a decrease of the fibers' diameter and an increase of the mesoscopic roughness since the

Table 1. Specific Surface Areas, Total Pore Volume, and Surface Roughness of the Calcined TiO_2 Fibers Obtained through Nitrogen Physisorption Experiments

fibers	BET surface ($m^2 \cdot g^{-1}$)	BJH surface[a] ($m^2 \cdot g^{-1}$)	total pore volume ($mL \cdot g^{-1}$)	D_s (surface roughness)
TiO_2	91	110	0.16	2.54
130-10-TiO_2	92	110	0.13	2.53
130-30-TiO_2	92	110	0.14	2.55
130-60-TiO_2	88	106	0.14	2.50
260-10-TiO_2	89	106	0.14	2.54
260-30-TiO_2	96	116	0.15	2.52
260-60-TiO_2	95	112	0.15	2.50
TiO_2[a]ref	700	652	0.82	2.31

[a]"TiO_2 ref" refers to the reference.[50]

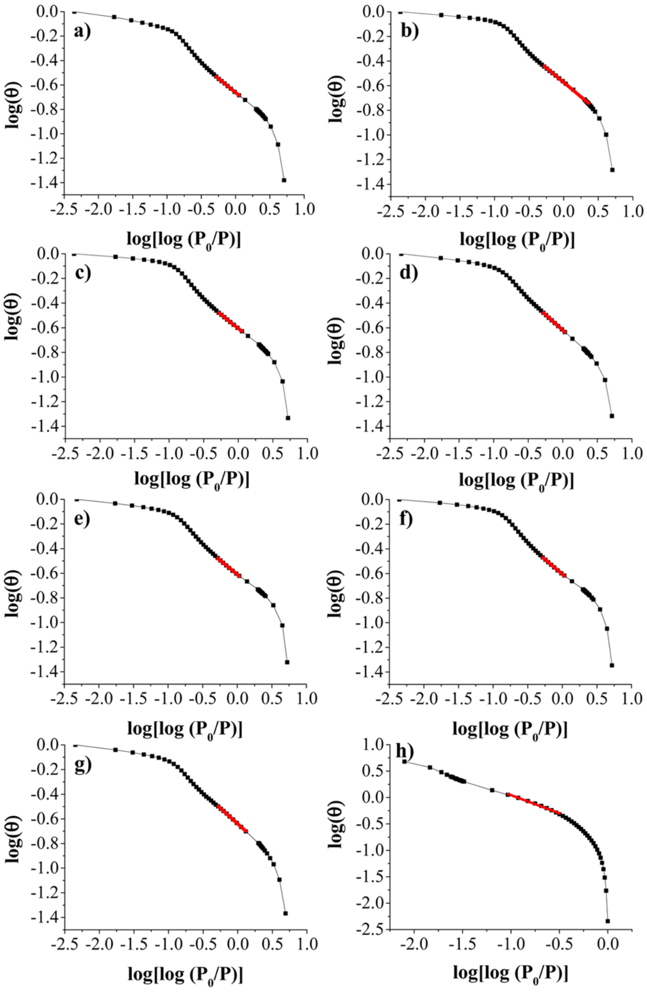

Figure 4. Surface fractal analysis of (a) TiO_2, (b) 130-10-TiO_2, (c) 130-30-TiO_2, (d) 130-60-TiO_2, (e) 260-10-TiO_2, (f) 260-30-TiO_2, (g) 260-60-TiO_2, and (h) TiO_2 ref fibers obtained from the adsorption curve of the isotherm.

roughness of the new fibers ($D_s = 2.5$) is much higher than the previous one ($D_s = 2.3$).

Considering the surface macroscopic topology, by comparing the TiO_2 fibers with and without latex prepared under these new conditions, it may be concluded that latex beads, used as sacrificial templates, induced an improvement of the efficiency for the fibers templated by 130 nm latex particles, but not for the one templated by 260 nm ones, except for the 260-60-TiO_2 sample. Regarding the 260 nm latex-based TiO_2 fibers, we observed that the increase of the latex content increased the efficiency of the fibers (Figure 5b). It also appeared that, for a given latex content, the fibers templated by 130 nm latex particles performed better than the 260 nm fibers, if the previously mentioned 130-60-TiO_2 sample was discarded. Generally, this difference in reaction kinetics can be attributed to a difference in the fibers' surface macroscopic topology, which leads to a better light penetration within the structure and to a turbulent-induced air flux behavior at the fibers' surface, favoring acetone degradation reaction. This result is important as it shows that the surface macroscopic topology is also a parameter to take into account when it comes to gas-based photocatalytic performances.

Regarding the mineralization percentage, it was calculated between 200 and 400 min of irradiation (Figure 5c) and was found to be stable in this range taking into account a significant error due to the addition of CO_2 and acetone leaks in the calculation. The mineralization percentage is varying from 46 (260-30-TiO_2) to 91% (130-60-TiO_2), with most of the fibers presenting a similar mineralization percentage around 70%. Two sets of fibers may be distinguished, presenting either a lower or a higher mineralization rate than the majority of the other fibers (Figure 5d). The first group, offering a lower mineralization rate, is composed of the 260-10-TiO_2 and 260-30-TiO_2 fibers, which is consistent with what we observed for the acetone degradation kinetics. From this result, we can deduce that insertion of voids created by large latex particles in small proportion does not allow optimizing both mesoscopic roughness and macroscopic topological defects to promote long residence time of acetone on the fibers' surface and thereby efficient mineralization. However, by increasing their concentration (260-60-TiO_2), it is possible to optimize these two morphological characteristics for a better residence time, more turbulent hydrodynamic gas flux character, and thus a better mineralization rate. The second group, which presents a higher mineralization rate than the majority of the fibers, is composed of the 130-60-TiO_2 fibers. From this result, we can conclude that the surface macroscopic topology created by small latex particles at high concentration (succession of medium pores inside the structure) permits also increasing the time of residence of acetone onto the TiO_2 fibers surface and thereby the mineralization process.

To summarize, we can say that morphological characteristics such as fiber diameters, mesoscopic surface roughness, and macroscopic topology are acting cooperatively toward both acetone degradation kinetics and its mineralization process. These above-mentioned morphological parameters should be regarded also as important factors deeply involved toward the efficiency of gas-phase photocatalysis.

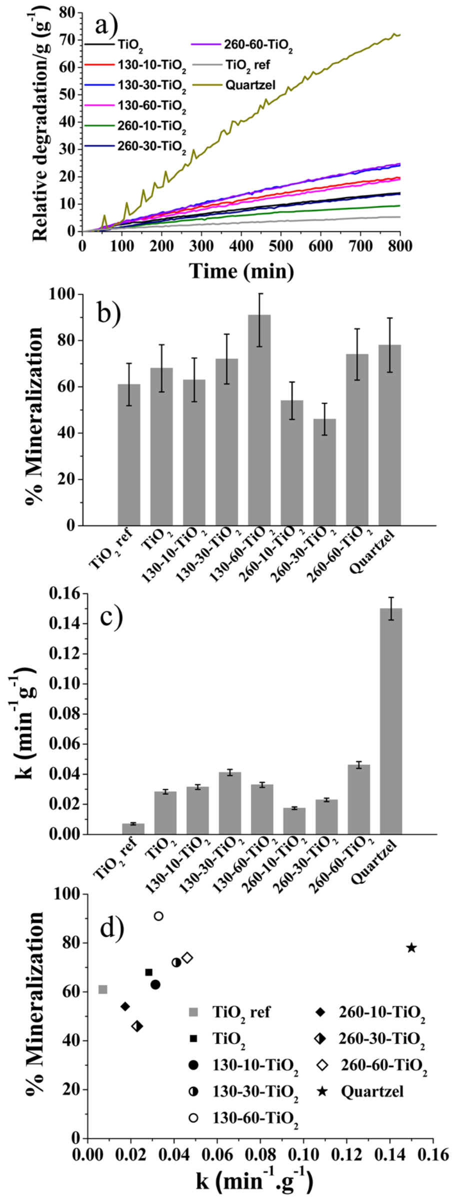

Figure 5. Results for the photocatalytic properties of the fibers: (a) % acetone degradation/g of media against time; the mass of media employed is proposed in Table S.1 (Supporting Information). (b) % mineralization between 200 and 400 min. (c) Pseudo-first-order rate constants of acetone degradation calculated from the degradation rate by gram of media. (d) Comparison between acetone degradation %/g media relative to % mineralization for the seven types of fibers, the reference fibers, and Quartzel fibers under irradiation of gaseous acetone at 366 nm (RH 15%, temperature 22 ± 2 °C, initial acetone concentration 50 ppmv, air flow rate 3.3 L·min^{-1}).

■ CONCLUSION

In this study, we have employed the extrusion process to promote the morphosyntheses of hybrid titania-based macroscopic fibers. Within the starting sols, we have varied both the diameters of the latex nanoparticles in use as well as their concentration. Upon a thermal treatment in air, we obtained the anatase phase of TiO_2 with residual brookite, while the latex calcination allows promoting tunable voids. Increasing the fibers' mesoscopic roughness and decreasing the fibers' diameter allow enhancing the fibers' efficiency toward acetone degradation. Moreover, by modifying the fiber surface macroscopic topologies, the acetone degradation kinetics is multiplied by 1.64, which represents a total increase of the reaction kinetics by a factor 6.5 compared to previous work. We proposed that the fiber diameters, mesoscopic roughness, and macroscopic topological defects are key parameters acting cooperatively for acetone degradation and mineralization processes. These morphological characteristics should certainly be added to the list of the already admitted key parameters (particle sizes, crystalline character, surface area) involved in the air-photocatalysis efficiency.

Despite this increase of air-phase photocatalytic efficiency, the best fibers generated in this study are still less active than the commercial Quartzel titania-based photocatalyst, being 3 times less efficient relative to the acetone degradation rate while offering the approximately same mineralization capabilities. The big first penalty of the fibers synthesized in this work is that their thickness does not allow optimizing the quantity of matter in interaction with the UV light penetration depth, most of the fibers being indeed not active. As all the catalytic efficiencies toward both acetone degradation and associated mineralization are normalized per gram of media, this feature is of crucial importance. The second main issue is of technology, when regarding the extrusion process, making use of a rotating beaker. This configuration, well calibrated for lab experiments, does not allow for higher scale industrial production. Our goal is to cancel the two above-mentioned penalties at once, this is to say, minimizing the fiber diameter as low as possible while offering a technological process able to address high scale industrial production, several hundred meters of TiO_2 fibers at once.

■ ASSOCIATED CONTENT

Ⓢ Supporting Information

Photocatalytic circulating batch in use, X-ray diffraction patterns of the fibers after calcination, kinetics reactions obtained through photocatalytic experiments, and mass of the as-synthesized TiO_2 fibers used for the photocatalysis experiments. This material is available free of charge via the Internet at http://pubs.acs.org.

■ AUTHOR INFORMATION

Corresponding Authors

*Phone: +33 559 407 579. Fax: +33 559 407 622. E-mail: sylvie.lacombe@univ-pau.fr (S.L.).
*Phone: +33 556 845630. Fax: 33 556 845600. E-mail: backov@crpp-bordeaux.cnrs.fr (R.B.).

Notes

The authors declare no competing financial interest.

■ REFERENCES

(1) Tang, X.; Li, D. Evaluation of Asphaltene Degradation on Highly Ordered TiO_2 Nanotubular Arrays via Variations in Wettability. *Langmuir* **2011**, *27*, 1218−1223.

(2) Naik, G. K.; Mishra, P. M.; Parida, K. Green Synthesis of Au/TiO_2 for Effective Dye Degradation in Aqueous System. *Chem. Eng. J.* **2013**, *229*, 492−497.

(3) Jiang, X.; Wang, T. Influence of Preparation Method on Morphology and Photocatalysis Activity of Nanostructured TiO_2. *Environ. Sci. Technol.* **2007**, *41*, 4441−4446.

(4) Zhang, R.; Tu, B.; Zhao, D. Synthesis of Highly Stable and Crystalline Mesoporous Anatase by Using a Simple Surfactant Sulfuric Acid Carbonization Method. *Chem.—Eur. J.* **2010**, *16*, 9977−9981.

(5) Ren, Y.; Chen, M.; Zhang, Y.; Wu, L. Fabrication of Rattle-Type TiO_2/SiO_2 Core/Shell Particles with Both High Photoactivity and UV-Shielding Property. *Langmuir* **2010**, *26*, 11391−11396.

(6) Chen, D.; Caruso, R. A. Recent Progress in the Synthesis of Spherical Titania Nanostructures and Their Applications. *Adv. Funct. Mater.* **2013**, *23*, 1356−1374.

(7) Carp, O.; Huisman, C. L.; Releer, A. Photoinduced Reactivity of Titanium Dioxide. *Prog. Solid State Chem.* **2004**, *32*, 33−177.

(8) Li, X.; John, V. T.; He, G.; Zhan, J.; Tan, G.; McPherson, G.; Bose, A.; Sarkar, J. Shear Induced Formation of Patterned Porous Titania with Applications to Photocatalysis. *Langmuir* **2009**, *25*, 7586−7593.

(9) Kim, D. S.; Han, S. J.; Kwak, S.-Y. Synthesis and Photocatalytic Activity of Mesoporous TiO_2 with the Surface Area, Crystallite Size, and Pore Size. *J. Colloid Interface Sci.* **2007**, *316*, 85−91.

(10) Zhao, B.; Lin, L.; He, D. Phase and Morphological Transitions of Titania/Titanate Nanostructures from an Acid to an Alkali Hydrothermal Environment. *J. Mater. Chem. A* **2013**, *1*, 1659−1668.

(11) Lee, M.; Amaratunga, P.; Kim, J.; Lee, D. TiO_2 Nanoparticle Photocatalysts Modified with Monolayer-Protected Gold Clusters. *J. Phys. Chem. C* **2010**, *114*, 18366−18371.

(12) Ohtani, B. Photocatalysis A to Z—What We Know and What We Do Not Know in a Scientific Sense. *J. Photochem. Photobiol., C* **2010**, *11*, 157−178.

(13) Henderson, M. A. A Surface Science Perspective on TiO_2 Photocatalysis. *Surf. Sci. Rep.* **2011**, *66*, 185−297.

(14) Mohapatra, P.; Mishra, T.; Parida, K. Effect of Microemulsion Composition on Textural and Photocatalytic Activity of Titania Nanomaterial. *Appl. Catal., A* **2006**, *310*, 183−189.

(15) Li, W.; Wu, Z.; Wang, J.; Elzatahry, A. A.; Zhao, D. A Perspective on Mesoporous TiO_2 Materials. *Chem. Mater.* **2014**, *26*, 287−298.

(16) Liu, R.; Ren, Y.; Shi, Y.; Zhang, F.; Zhang, L.; Tu, B. Controlled Synthesis of Ordered Mesoporous C-TiO_2 Nanocomposites with Crystalline Titania Frameworks from Organic-Inorganic-Amphiphilic Coassembly. *Chem. Mater.* **2008**, *20*, 1140−1146.

(17) Kasuga, B. T.; Hiramatsu, M.; Hoson, A.; Sekino, T.; Niihara, K. Titania Nanotubes Prepared by Chemical Processing. *Adv. Mater.* **1999**, *11*, 1307−1311.

(18) Liu, S. M.; Gan, L. M.; Liu, L. H.; Zhang, W. D.; Zeng, H. C. Synthesis of Single-Crystalline TiO_2 Nanotubes. *Chem. Mater.* **2002**, *14*, 1391−1397.

(19) Zhang, L.; Yu, J. C. A Sonochemical Approach to Hierarchical Porous Titania Spheres with Enhanced Photocatalytic Activity. *Chem. Commun.* **2003**, 2078−2079.

(20) Shibata, H.; Ogura, T.; Mukai, T.; Ohkubo, T.; Sakai, H.; Abe, M. Direct Synthesis of Mesoporous Titania Particles Having a Crystalline Wall. *J. Am. Chem. Soc.* **2005**, *127*, 16396−16397.

(21) Yuan, Z.-Y.; Ren, T.-Z.; Vantomme, A.; Su, B.-L. Facile and Generalized Preparation of Hierarchically Mesoporous−Macroporous Binary Metal Oxide Materials. *Chem. Mater.* **2004**, *16*, 5096−5106.

(22) On, D. T. A Simple Route for the Synthesis of Mesostructured Lamellar and Hexagonal Phosphorus-Free Titania (TiO_2). *Langmuir* **1999**, *15*, 8561−8564.

(23) Antonelli, D. M. Synthesis of Phosphorus-Free Mesoporous Titania via Templating with Amine Surfactants. *Microporous Mesoporous Mater.* **1999**, *30*, 315−319.

(24) Yun, H.; Miyazawa, K.; Zhou, H.; Honma, I.; Kuwabara, M. Synthesis of Mesoporous Thin TiO_2 Films with Hexagonal Pore Structures Using Triblock Copolymer Templates. *Adv. Mater.* **2001**, *13*, 1377−1380.

(25) Yuan, Z.-Y.; Ren, T.-Z.; Su, B.-L. Hierarchically Mesostructured Titania Materials with an Unusual Interior Macroporous Structure. *Adv. Mater.* **2003**, *15*, 1462−1465.

(26) Zhou, Y.; Antonietti, M. Synthesis of Very Small TiO_2 Nanocrystals in a Room-Temperature Ionic Liquid and Their Self-Assembly toward Mesoporous Spherical Aggregates. *J. Am. Chem. Soc.* **2003**, *125*, 14960−14961.

(27) Blin, J.-L.; Léonard, A.; Yuan, Z.-Y.; Gigot, L.; Vantomme, A.; Cheetham, A. K.; Su, B.-L. Hierarchically Mesoporous/Macroporous Metal Oxides Templated from Polyethylene Oxide Surfactant Assemblies. *Angew. Chem., Int. Ed.* **2003**, *42*, 2872−2875.

(28) Coakley, K. M.; Liu, Y.; McGehee, M. D.; Frindell, K. L.; Stucky, G. D. Infiltrating Semiconducting Polymers into Self-Assembled Mesoporous Titania Films for Photovoltaic Applications. *Adv. Funct. Mater.* **2003**, *13*, 301−306.

(29) Antonelli, D. M.; Ying, J. Y. Synthesis of Hexagonally Packed Mesoporous TiO_2 by a Modified Sol-Gel Method. *Angew. Chem., Int. Ed. Engl.* **1995**, *34*, 2014−2017.

(30) Wang, K.; Yao, B.; Morris, M. a.; Holmes, J. D. Supercritical Fluid Processing of Thermally Stable Mesoporous Titania Thin Films with Enhanced Photocatalytic Activity. *Chem. Mater.* **2005**, *17*, 4825−4831.

(31) Kirsch, B. L.; Richman, E. K.; Riley, A. E.; Tolbert, S. H. In-Situ X-ray Diffraction Study of the Crystallization Kinetics of Mesoporous Titania Films. *J. Phys. Chem. B* **2004**, *108*, 12698−12706.

(32) Liu, Z.; Sun, D. D.; Guo, P.; Leckie, J. O. An Efficient Bicomponent TiO_2/SnO_2 Nanofiber Photocatalyst Fabricated by Electrospinning with a Side-by-Side Dual Spinneret Method. *Nano Lett.* **2007**, *7*, 1081−1085.

(33) Zhang, Y. X.; Li, G. H.; Jin, Y. X.; Zhang, Y.; Zhang, J.; Zhang, L. D. Hydrothermal Synthesis and Photoluminescence of TiO_2 Nanowires. *Chem. Phys. Lett.* **2002**, *365*, 300−304.

(34) Kelly, S.; Pollak, F. H.; Tomkiewicz, M. Raman Spectroscopy as a Morphological Probe for TiO_2 Aerogels. *J. Phys. Chem. B* **1997**, *101*, 2730−2734.

(35) Zhang, W. F.; He, Y. L.; Zhang, M. S.; Yin, Z.; Chen, Q. Raman Scattering Study on Anatase TiO_2 Nanocrystals. *J. Phys. D: Appl. Phys.* **2000**, *33*, 912−916.

(36) Bannat, I.; Wessels, K.; Oekermann, T.; Rathousky, J.; Bahnemann, D.; Wark, M. Improving the Photocatalytic Performance of Mesoporous Titania Films by Modification with Gold Nanostructures. *Chem. Mater.* **2009**, *21*, 1645−1653.

(37) Innocenzi, P.; Malfatti, L.; Soler-Illia, G. J. A. A. Hierarchical Mesoporous Films: From Self-Assembly to Porosity with Different Length Scales. *Chem. Mater.* **2011**, *23*, 2501−2509.

(38) Shchukin, D.; Sviridov, D. Photocatalytic Processes in Spatially Confined Micro- and Nanoreactors. *J. Photochem. Photobiol., C* **2006**, *7*, 23−39.

(39) Madhugiri, S.; Sun, B.; Smirniotis, P. G.; Ferraris, J. P.; Balkus, K. J. Electrospun Mesoporous Titanium Dioxide Fibers. *Microporous Mesoporous Mater.* **2004**, *69*, 77−83.

(40) Nuansing, W.; Ninmuang, S.; Jarernboon, W.; Maensiri, S.; Seraphin, S. Structural Characterization and Morphology of Electrospun TiO_2 Nanofibers. *Mater. Sci. Eng., B* **2006**, *131*, 147−155.

(41) Aprile, C.; Corma, A.; Garcia, H. Enhancement of the Photocatalytic Activity of TiO_2 through Spatial Structuring and Particle Size Control: From Subnanometric to Submillimetric Length Scale. *Phys. Chem. Chem. Phys.* **2008**, *10*, 769−783.

(42) Caruso, R. A.; Schattka, J. H.; Greiner, A. Titanium Dioxide Tubes from Sol-Gel Coating of Electrospun Polymer Fibers. *Adv. Mater.* **2001**, *13*, 1577−1579.

(43) Lei, Y.; Zhang, L. D.; Meng, G. W.; Li, G. H.; Zhang, X. Y.; Liang, C. H.; Chen, W.; Wang, S. X. Preparation and Photoluminescence of Highly Ordered TiO_2 Nanowire Arrays. *Appl. Phys. Lett.* **2001**, *78*, 1125−1127.

(44) Xiang, B.; Zhang, Y.; Wang, Z.; Luo, X. H.; Zhu, Y. W.; Zhang, H. Z.; Yu, D. P. Field-Emission Properties of TiO_2 Nanowire Arrays. *J. Phys. D: Appl. Phys.* **2005**, *38*, 1152−1155.

(45) Backov, R. Combining Soft Matter and Soft Chemistry: Integrative Chemistry towards Designing Novel and Complex Multiscale Architectures. *Soft Matter* **2006**, *2*, 452−464.

(46) Prouzet, E.; Khani, Z.; Bertrand, M.; Tokumoto, M.; Guyot-Ferreol, V.; Tranchant, J.-F. An Example of Integrative Chemistry: Combined Gelation of Boehmite and Sodium Alginate for the Formation of Porous Beads. *Microporous Mesoporous Mater.* **2006**, *96*, 369−375.

(47) Prouzet, E.; Ravaine, S.; Sanchez, C.; Backov, R. Bio-inspired Synthetic Pathways and beyond: Integrative Chemistry. *New J. Chem.* **2008**, *32*, 1284−1299.

(48) Brun, N.; Ungureanu, S.; Deleuze, H.; Backov, R. Hybrid Foams, Colloids and beyond: From Design to Applications. *Chem. Soc. Rev.* **2011**, *40*, 771−788.

(49) Nicole, L.; Rozes, L.; Sanchez, C. Integrative Approaches to Hybrid Multifunctional Materials: From Multidisciplinary Research to Applied Technologies. *Adv. Mater.* **2010**, *22*, 3208−3214.

(50) Kinadjian, N.; Le Bechec, M.; Pigot, T.; Dufour, F.; Durupthy, O.; Bentaleb, A.; Prouzet, E.; Lacombe, S.; Backov, R. Photocatalytic TiO_2 Macroscopic Fibers Obtained Through Integrative Chemistry. *Eur. J. Inorg. Chem.* **2012**, 5350−5359.

(51) Biette, L.; Carn, F.; Maugey, M.; Achard, M.-F.; Maquet, J.; Steunou, N.; Livage, J.; Serier, H.; Backov, R. Macroscopic Fibers of Oriented Vanadium Oxide Ribbons and Their Application as Highly Sensitive Alcohol Microsensors. *Adv. Mater.* **2005**, *17*, 2970−2974.

(52) Serier, H.; Achard, M.-F.; Babot, O.; Steunou, N.; Maquet, J.; Livage, J.; Leroy, C. M.; Backov, R. Designing the Width and Texture of Vanadium Oxide Macroscopic Fibers: Towards Tuning Mechanical Properties and Alcohol-Sensing Performance. *Adv. Funct. Mater.* **2006**, *16*, 1745−1753.

(53) Dexmer, J.; Leroy, C. M.; Binet, L.; Heresanu, V.; Launois, P.; Steunou, N.; Coulon, C.; Maquet, J.; Brun, N.; Livage, J.; Backov, R. Vanadium Oxide−PANI Nanocomposite-Based Macroscopic Fibers: 1D Alcohol Sensors Bearing Enhanced Toughness. *Chem. Mater.* **2008**, *20*, 5541−5549.

(54) Leroy, M.; Achard, M.; Babot, O.; Steunou, N.; Masse, P.; Livage, J.; Binet, L.; Brun, N. Designing Nanotextured Vanadium Oxide-Based Macroscopic Fibers: Application as Alcoholic Sensors. *Chem. Mater.* **2007**, *19*, 3988−3999.

(55) Brun, N.; Leroy, C. M.; Dexmer, J.; Serier, H.; Carn, F.; Biette, L.; Backov, R. Integrative Chemistry Portfolio toward Designing and Tuning Vanadium Oxide Macroscopic Fibers Sensing and Mechanical Properties. *C. R. Chim.* **2010**, *13*, 154−166.

(56) Kinadjian, N.; Achard, M.; Julián-lópez, B.; Maugey, M.; Poulin, P.; Prouzet, E.; Backov, R. ZnO/PVA Macroscopic Fibers Bearing Anisotropic Photonic Properties. *Adv. Funct. Mater.* **2012**, *22*, 3994−4003.

(57) Zhang, J.; Chen, Z.; Wang, Z.; Zhang, W.; Ming, N. Preparation of Monodisperse Polystyrene Spheres in Aqueous Alcohol System. *Mater. Lett.* **2003**, *57*, 4466−4470.

(58) Avnir, D.; Jaroniec, M. An Isotherm Equation for Adsorption on Fractal Surfaces of Heterogeneous Porous Materials. *Langmuir* **1989**, *5*, 1431−1433.

(59) Prouzet, E.; Boissière, C.; Kim, S. S.; Pinnavaia, T. J. Roughness of Mesoporous Silica Surfaces Deduced from Adsorption Measurements. *Microporous Mesoporous Mater.* **2009**, *119*, 9−17.

(60) Rouquerol, J.; Avnir, D.; Fairbridge, C. W.; Everett, D. H.; Haynes, J. H.; Pernicone, N.; Ramsay, J. D. F.; Sing, K. S. W.; Unger, K. K. Recommendations for the Characterization of Porous Solids. *Pure Appl. Chem.* **1994**, *66*, 1739−1758.

(61) Peral, J.; Ollis, D. F. Heterogeneous Photocatalytic Oxidation of Gas-Phase Organics for Air Purification: Acetone, 1-Butanol, Butyraldehyde, Formaldehyde, and *m*-Xylene Oxidation. *J. Catal.* **1992**, *136*, 554−565.

(62) Besov, A. S.; Vorontsov, A. V. Fast Elimination of Organic Airborne Compounds by Adsorption and Catalytic Oxidation over Aerosol TiO_2. *Catal. Commun.* **2008**, *9*, 2598−2600.

(63) Vincent, G.; Marquaire, P. M.; Zahraa, O. Abatement of Volatile Organic Compounds Using an Annular Photocatalytic Reactor: Study of Gaseous Acetone. *J. Photochem. Photobiol., A* **2008**, *197*, 177−189.

(64) Yu, J.; Zhang, L.; Cheng, B.; Su, Y. Hydrothermal Preparation and Photocatalytic Activity of Hierarchically Sponge-like Macro-/Mesoporous Titania. *J. Phys. Chem. C* **2007**, *111*, 10582−10589.

(65) Neti, N. R.; Parnar, G. R.; Bakardjeva, S.; Subrt, J. Thick Film Titania on Glass Supports for Vapour Phase Photocatalytic Degradation of Toluene, Acetone, and Ethanol. *Chem. Eng. J.* **2010**, *163*, 219−229.